eds.), 686, Univ. of Arizona, Tucson. [3] Bell J. (1992) *Icarus, 100,* 575. [4] Erard S. et al. (1991) *LPS XXI,* 437. [5] Bibring J.-P. et al. (1990) *LPS XX,* 461. [6] Murchie S. et al. (1992) *LPS XXIII,* 941. [7] Mustard J. et al. (1993) *LPS XXIV,* 1039. [8] Murchie S. et al. (1993) *Icarus,* in press. [9] Palluconi F. and Kieffer H. (1978) *Icarus, 45,* 415. [10] Christensen P. (1986) *Icarus, 68,* 217. [11] Morris R. et al. (1985) *JGR, 90,* 3126. [12] Singer R. and Roush T. (1983) *LPS XIV,* 708. [13] Morris R. and Neely S. (1982) *LPS XIII,* 548. [14] Merenyi E. et al. (1992) *LPS XXIII,* 897. [15] Grizzaffi P. and Schultz P. (1989) *Icarus, 77,* 358. [16] Geissler P. et al. (1993) *Icarus,* in press. [17] Witbeck N. et al. (1991) *U.S.G.S. Misc. Inv. Ser. Map I-2010.* [18] Komatsu G. et al. (1993) *JGR. 98.* 11105.

N94-33221

531-91 ABS. ONLY 427043

EDDY TRANSPORT OF WATER VAPOR IN THE MARTIAN ATMOSPHERE.

J. R. Murphy[1,2] and R. M. Haberle[1], [1]SJSU Foundation, [2]NASA Ames Research Center, Moffett Field CA 94035, USA.

Viking orbiter measurements of the martian atmosphere suggest that the residual north polar water-ice cap is the primary source of atmospheric water vapor, which appears at successively lower northern latitudes as the summer season progresses [1]. Zonally symmetric studies of water vapor transport indicate that the zonal mean meridional circulation is incapable (due to its weakness at high latitudes) of transporting from north polar regions to low latitudes the quantity of water vapor observed [2]. This result has been interpreted as implying the presence of nonpolar sources of water, namely subsurface ice and adsorbed water, at northern middle and subtropical latitudes. Another possibility, which has not been explored, is the ability of atmospheric wave motions, which are not accounted for in a zonally symmetric framework, to efficiently accomplish the transport from a north polar source to the entirety of the northern hemisphere. The ability or inability of the full range of atmospheric motions to accomplish this transport has important implications regarding the questions of water sources and sinks on Mars: if the full spectrum of atmospheric motions proves to be incapable of accomplishing the transport, it strengthens arguments in favor of additional water sources.

Preliminary results from a three-dimensional atmospheric dynamical/water vapor transport numerical model will be presented. The model accounts for the physics of a subliming water-ice cap, but does not yet incorporate recondensation of this sublimed water. Transport of vapor away from this water-ice cap in this three-dimensional framework will be compared with previously obtained zonally symmetric (two-dimensional) results to quantify effects of water vapor transport by atmospheric eddies.

References: [1] Jakosky and Farmer (1982) *JGR, 87,* 2999–3019. [2] Haberle and Jakosky (1990) *JGR, 95,* 1423–1437.

N94-33222

531-91 ABS.

IRTM BRIGHTNESS TEMPERATURE MAPS OF THE MARTIAN SOUTH POLAR REGION DURING THE POLAR NIGHT: THE COLD SPOTS DON'T MOVE.

D. A. Paige[1], D. Crisp[2], M. L. Santee[2], and M. I. Richardson[1], [1]Department of Earth and Space Sciences, UCLA, Los Angeles CA 90024, USA, [2]Jet Propulsion Laboratory, Pasadena CA 91106, USA.

The Viking Infrared Thermal Mapper (IRTM) polar winter season observations in the 20-μm channel showed considerable temporal and spatial structure, with minimum brightness temperatures well below the surface CO_2 frost point of ~148 K [1,2]. Brightness temperatures as low as 134 K in the south and 128 K in the north were observed. To date, these low brightness temperatures have not been uniquely explained. In the 1976 paper, Kieffer et al. [1] suggested three mechanisms: (1) low surface emissivities, (2) presence of high-altitude clouds, and (3) depressed solid-vapor equilibrium CO_2 frost kinetic temperatures due to reduced atmospheric CO_2 partial pressures at the surface. Hess [3] cast doubt on mechanism (3) by showing that vertical and horizontal gradients in average molecular weight of the polar atmosphere could only be stable under special circumstances.

In 1979, Ditteon and Kieffer [4] published infrared transmission spectra of thick, solid CO_2 samples grown in the laboratory. The results showed that in wavelengths away from the strong CO_2 absorption features, the transmissivity of their samples was quite high, and concluded that the low brightness temperature observations could be explained by low surface frost emissivity. Warren et al. [5] have used Ditteon and Kieffer's laboratory data in conjunction with scattering models to show that the spectral emissivities of martian CO_2 frosts could take on almost any value from 0 to 1 depending on CO_2 grain size, dust and water ice content, or viewing angle.

Hunt [6] showed that the polar night brightness temperatures could be explained by the radiative effects of CO_2 clouds. Using the results of a one-dimensional atmospheric model in conjunction with IRTM observations, Paige [7,8] showed that the spatial and temporal occurrence of low brightness temperatures are consistent with the notion that they are due to CO_2 clouds. Subsequently, Pollack et al. [9] published the results of Global Circulation Model (GCM) experiments that showed that CO_2 should condense in the atmosphere over the winter pole and that this condensation is enhanced by the presence of dust.

In the 1977 paper, Kieffer et al. [2] published midwinter brightness temperature maps that showed some evidence of temporal variation. These temporal variations have since been interpreted by others as illustrating dynamic motions of the lowest of the low brightness temperature regions. However, Kieffer et al. [2] state that the possible motion of individual features cannot be established from the analysis presented in the 1977 paper.

In this study, we have examined a series of IRTM south polar brightness temperature maps obtained by Viking Orbiter 2 during a 35-day period during the southern fall season in 1978 (L_s 47.3 to 62.7, Julian Date 2443554 to 2443588). These maps represent the best spatial and temporal coverage obtained by IRTM during a polar-night season that have not been analyzed in previous studies. The maps show a number of phenomena that have been identified in previous studies, including day-to-day brightness temperature variations in individual low-temperature regions [1], and the tendency for

IRTM 11-μm channel brightness temperatures to also decrease in regions where low 20-μm channel brightness temperatures are observed [7,8]. The maps also show new phenomena, the most striking of which is a clear tendency for the low-brightness temperature regions to occur at fixed geographic locations. During this season, the coldest low brightness temperatures appear to be concentrated in distinct regions, with spatial scales ranging from 50 to 300 km. There are approximately a dozen of these concentrations, with the largest centered near the location of the south residual polar cap. Other concentrations are located at Cavi Angusti, and close to the craters Main, South, Lau, and Dana. Broader, less-intense regions appear to be well correlated with the boundaries of the south polar layered deposits, and the Mountains of Mitchell. We have thus far detected no evidence for horizontal motion of any of these regions.

The fact that the low brightness temperature regions do not appear to move and are correlated with the locations of surface features suggests that they are not artifacts of the IRTM instrument or its viewing geometry, but the result of processes occurring on the surface or in the lower atmosphere. Presently, we do not know whether other low brightness temperature regions that have been observed during the southern winter or during the northern fall and winter exhibit similar spatial and temporal behavior. We intend to better understand the cause(s) and implications of these phenomena through modeling and further analysis of the Viking and Mariner 9 datasets.

References: [1] Kieffer H. H. et al. (1976) *Science, 193*, 780–786. [2] Kieffer H. H. et al. (1977) *JGR, 82*, 4249–4291. [3] Hess S. L. (1979) *JGR, 84*, 2969–2973. [4] Ditteon R. and Kieffer H. H. (1979) *JGR, 84*, 8294–8300. [5] Warren S. G. et al. (1990) *JGR, 95*, 14717–14741. [6] Hunt G. E. (1980) *GRL, 7*, 481–484. [7] Paige D. A. (1985) Ph.D. thesis, California Institute of Technology. [8] Paige D. A. and Ingersoll A. P. (1985) *Science, 228*, 1160–1168. [9] Pollack J. B. et al. (1990) *JGR, 94*, 1447–1473.

533-91 ABS. 01 **N94-33223**

NUMERICAL SIMULATION OF THERMALLY INDUCED NEAR-SURFACE FLOWS OVER MARTIAN TERRAIN.

T. R. Parish[1] and A. D. Howard[2], [1]Department of Atmospheric Science, University of Wyoming, Laramie WY 82071, USA, [2]Department of Environmental Sciences, University of Virginia, Charlottesville VA 22903, USA.

Introduction: The near-surface martian wind and temperature regimes display striking similarities to terrestrial desert counterparts [1,2]. The diurnal radiative cycle is responsible for establishment of a pronounced thermal circulation in which downslope (katabatic) flows prevail during the nighttime hours and weak upslope (anabatic) conditions prevail during the daytime. The low-level wind regime appears to play an important role in modifying the surface of the polar regions [3]. Viking imagery of the north polar cap shows evidence of eolian characteristics such as dunes, frost streaks, and wind-scour features. The direction of the prevailing wind can in cases be inferred from the orientation of surface features such as frost streaks and ice grooves.

For the past several years a numerical modeling study has been in progress to examine the sensitivity of thermally induced surface winds on Mars to the patterns of solar insolation and longwave radiative. The model used is a comprehensive atmospheric mesoscale equation system that has been employed previously for simulation of Antarctic katabatic winds [4]. The model equations are written in terrain-following sigma coordinates to allow for irregular terrain [5]; prognostic equations include the flux forms of

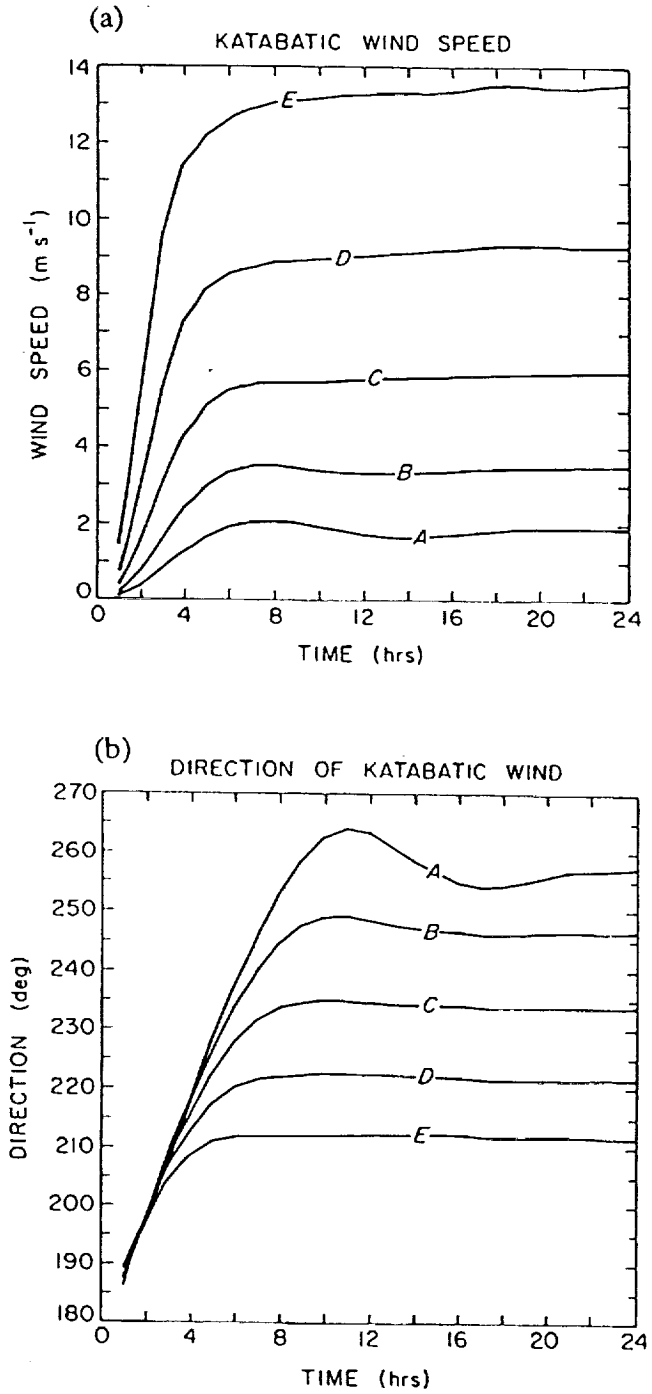

Fig. 1. Time evolution of (a) wind speed and (b) wind direction at the lowest sigma level (20 m) after 24-hr integration of constant slope runs for terrain slopes of 0.0005, 0.001, 0.002, 0.004, and 0.008, corresponding to curves A, B, C, D, and E respectively.